EXTENDED KINEMATIC MODEL OF THE 3-RPS SPATIAL PARALLEL MANIPULATOR

Sean A. Dowling, Juan A. Carretero
Department of Mechanical Engineering, University of New Brunswick, Fredericton, NB, Canada
Email: sean.a.dowling@gmail.com; Juan.Carretero@unb.ca

ABSTRACT

This paper presents the extended kinematic model of the 3-RPS spatial parallel manipulator. Starting from the accepted idealized model, a set of error parameters are introduced to accommodate all significant sources of disparity between the math model and actual kinematics of a real manipulator. This error set is incorporated into the vector loop equations locating the spherical joints at the end effector. As a result, the numerical solutions can then presented for both the extended forward and inverse displacement problems. The paper concludes with a parametric study on the effects of each error component on representative manipulator geometry in the presence of errors as well as without.

Keywords: 3-RPS; parallel manipulator; kinematics; extended model.

MODÈLE CINÉMATIQUE COMPLET DU MANIPULATEUR PARALLÈLE SPATIALE DE TYPE 3-RPS

RÉSUMÉ

Cet article présente le modèle cinématique complet du manipulateur parallèle spatial de type 3-RPS . A partir du modèle idéalisé, un ensemble de paramètres d'erreur est introduit pour tenir compte de toutes les sources importantes de disparité entre le modèle mathématique et les déplacements réel cinématique d'un manipulateur réel. Ces erreurs sont alors intégrées dans les équations de vecteur de boucle de positionnement des articulations sphériques à la nacelle. Et c'est ainsi que les solutions numériques sont ensuite présentées pour le problème géométrique direct et le problèmes géométrique inverse. Le document se termine par une étude paramétrique sur les effets de chaque composante d'erreur de manipulation de la géométrie représentant en présence d'erreurs aussi bien que sans.

Mots-clés : 3-RPS ; manipulateur parallèle ; modèle cinématique complet.

NOMENCLATURE

Base variables
$\{O'\}$	Mobile platform frame with origin at O'
A_i	Centre of spherical joint (mobile platform)
$\mathbf{a}_i$	Vector describing origin of $\{O\}$ to A_i (base link frame)
$\mathbf{a}'_i$	Vector describing origin of $\{O'\}$ to A_i (mobile platform frame)
r_p	Nominal radius containing all A_i (mobile platform frame)
$\{O\}$	Base link frame with origin at O
$\mathbf{p}$	Vector describing origin of $\{O\}$ to origin of $\{O'\}$ (base link frame)
B_i	Revolute/Prismatic joint intersection point location (base link)
$\mathbf{b}_i$	Vector describing origin of $\{O\}$ to B_i (base link frame)
r_b	Nominal radius containing all B_i (base link frame)
β_i	Angle between branches
λ_i	Revolute joint variable
q_i	Prismatic joint variable

Extended model specific variables
r_{pi}	Branch specific radial distance to A_i (mobile platform frame)
r_{bi}	Branch specific radial distance to B_i (base link frame)
α_i	Angle between branches (mobile platform frame)
ζ_i	Error angle defining amount revolute joint axis out of X-Y plane
κ_i	Error angle defining amount revolute joint axis out of perpendicularity with $\mathbf{b}_i$
γ_i	Error angle defining amount prismatic joint axis out of perpendicularity with revolute joint axis
δq_i	Prismatic joint offset

Parameter variation specific definitions
δr_{pi}	Branch specific error distance defining deviation from nominal radius r_p
δr_{bi}	Branch specific error distance defining deviation from nominal radius r_b
$\delta \alpha_i$	Branch specific error angle defining deviation from nominal branch angle α_i
$\delta \beta_i$	Branch specific error angle defining deviation from nominal branch angle β_i

1. INTRODUCTION

Following the debut of the Stewart-Gough platform [1], the field of Parallel Manipulators (PM) has been a topic of much interest covering a wide variety of configurations and applications. Compared to their serial counterparts, PM's are typically found in low inertia configurations with relatively high load capacity and stiffness. These benefits are not without penalty however and PMs are also typically characterised by limited workspaces and poor dexterity. Despite these shortcomings and working off their strengths, PMs have excelled in a number of industries and applications, including vehicle simulation [2], precision machining centres [3, 4] and haptic interfaces [5] to name just a few.

The particular configuration discussed herein is referred to as the 3-R$\underline{P}$S spatial PM first introduced by Hunt [6]. The configuration description given by 3-R$\underline{P}$S indicates that, from the base to the end-effector, each of the manipulator's three branches contains 1 **R**evolute (passive) joint, 1 **P**rismatic (actuated) joint and one **S**pherical (passive) joint. Following its introduction, this PM has been an area of active research with topics ranging from Jacobian/singularity analysis [7, 8], kinematics/dynamics synthesis [9, 10], workspace optimization and manipulator design [11, 12], as well as integration into larger robotic configurations [13].

While the first kinematic analysis of this PM was completed by Shah and Lee [14], the kinematic displacement problems made use of many assumptions regarding component alignment and assembly conditions to idealize the manipulator. Since this time, almost all research relating to this PM has made use of some variation of this idealized model. While some researchers have taken steps to improve upon this [15], the

work falls short in capturing all significant error components and is the primary motivation for the current research; to extend this model and more accurately represent the kinematics of the 3-R$\underline{P}$S.

To begin, the approximate kinematic model is developed using conventional methods along with both its forward and inverse displacement solutions. This is followed by a brief discussion on the number of architectural parameters required to build a comprehensive kinematic model for PMs and application of this theory to the 3-R$\underline{P}$S. The paper concludes with a parametric study on the effects of each error component on representative manipulator geometry in the presence of errors as well as without.

2. THE 3-R$\underline{P}$S MANIPULATOR

2.1. Description

The 3-R$\underline{P}$S spatial parallel manipulator comprises 3 identically configured branches connecting a base platform to a mobile platform. Each branch has 5 Degrees Of Freedom (DOF) containing 1 revolute joint, 1 prismatic joint and 1 spherical joint. For purposes of this research, both the revolute and spherical joints are defined as passive and without orientation feedback, while the connecting prismatic joint is defined active and assumed to have position data available. Based on this architecture and according to Chebychev-Grübler-Kutzbach (CGK) mobility formula, the resulting DOFs for the mechanism are:

$$F = 6(n - j - 1) + \sum_{i=1}^{j} f_i = 6(8 - 9 - 1) + 3(1 + 1 + 3) = 3$$

where n is the number of bodies in the mechanism, j is the number of joints and f_i is the number of DOFs associated with joint i. An implication of this result is that, while this manipulator is a spatial mechanism, only 3 of the 6 task-space variables are available as independent DOFs leaving the remaining 3 to be determined as functions of the user-selected independent variables.

The architectural parameters of the ideal kinematic model are shown schematically in Fig. 1 and reflect the variable set used during the forward and inverse displacement solutions for the ideal model.

2.2. Ideal (Approximate) Kinematic Model

In this ideal model, all three branches are considered identical. The points of intersection of the revolute joint axes and the line of action of the prismatic joints (B_i) form the points of an equilateral triangle, all residing on a circle of radius r_b whose centre is O. The revolute joint axes are all assumed to be at-once tangent to this circle and co-planar to the X-Y plane. The angles between branches 1 and 2 and branches 1 and 3 are denoted as β_2 and β_3 respectively with branch 1 aligned to the X-axis of $\{O\}$, thus $\beta_1 = 0$. It is then assumed that the corresponding branch angles of the mobile platform's spherical joints are also arranged in this fashion (i.e., $\alpha_i = \beta_i$) with joint centres A_i at radius r_p. As well, the line of action of the prismatic joint is assumed to be perpendicular to its respective revolute joint axis which as a result, restricts each spherical joint centre A_i to a plane perpendicular to the X-Y plane of $\{O\}$.

Remaining definitions from the vector model overlay of Fig. 1 show vector **p** describing a line connecting O to O' with the vectors $\mathbf{a}_i$ and $\mathbf{a}_i'$ describing lines passing through O, A_i and O', A_i, respectively. Finally, the vectors $\mathbf{b}_i$ define the set of lines passing through O and B_i.

2.2.1. Inverse Displacement Solution (IDS)

The purpose of the 3-R$\underline{P}$S IDS is to determine the prismatic joint lengths required to achieve a desired pose of the mobile platform. Conveniently, the IDS for the 3-R$\underline{P}$S is identical to that of the 3-$\underline{P}$RS developed in [11], making use of all the same assumptions detailed in section 2.2.

While the choice of which 3 task-space variables to select as independent is arbitrary, the variables used in [11] and [16] and most other papers dealing with the 3-$\underline{P}$RS or 3-R$\underline{P}$S manipulators will suffice for demon-
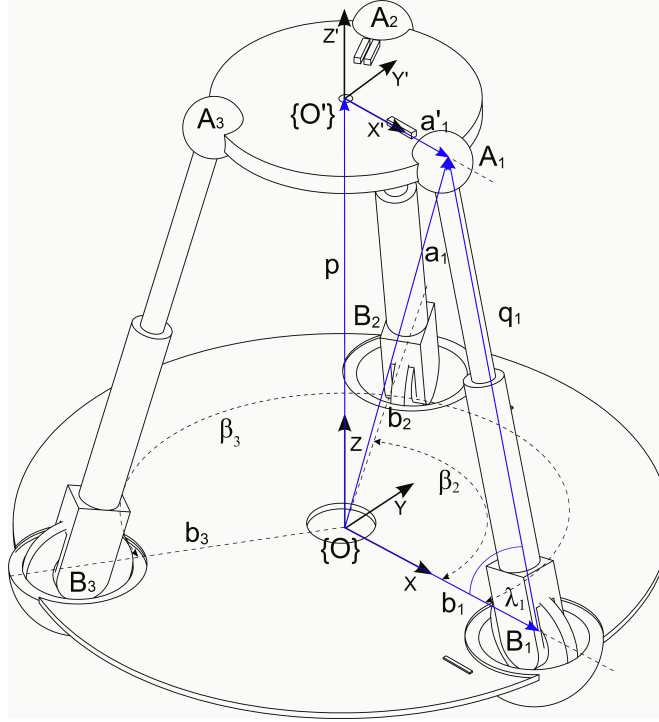
Fig. 1. Architectural parameters of the ideal 3-R$\underline{P}$S kinematic model.

stration purposes, namely: displacement along the inertial Z, and the tip and tilt angles of the mobile platform (rotations ψ and θ about the inertial X and Y axes respectively). As a result, this leaves displacements of the mobile platform in X and Y (often termed as parasitic), as well as rotation about Z (*i.e.*, ϕ) as dependent variables.

As shown below and detailed in [11], calculation of these dependent variables makes use of the vector loop equations depicted in Fig. 1 and many of the assumptions detailed in the ideal model description.

Given the following Euler angle rotation matrices:

$$\mathbf{R}_x(\theta) = \begin{bmatrix} 1 & 0 & 0 \\ 0 & cos(\theta) & -sin(\theta) \\ 0 & sin(\theta) & cos(\theta) \end{bmatrix}, \quad \mathbf{R}_y(\theta) = \begin{bmatrix} cos(\theta) & 0 & sin(\theta) \\ 0 & 1 & 0 \\ -sin(\theta) & 0 & cos(\theta) \end{bmatrix}, \quad \mathbf{R}_z(\theta) = \begin{bmatrix} cos(\theta) & -sin(\theta) & 0 \\ sin(\theta) & cos(\theta) & 0 \\ 0 & 0 & 1 \end{bmatrix}$$

and a coordinate system transformation sequence of:

$$
\begin{aligned}
\mathbf{T} &= \mathbf{T}_{ZXY} = \mathbf{R}_y(\theta)\mathbf{R}_x(\psi)\mathbf{R}_z(\phi) \\
&= \begin{bmatrix} c_\theta c_\phi + s_\psi s_\theta s_\phi & -c_\theta s_\phi + s_\psi s_\theta c_\phi & c_\psi s_\theta \\ c_\psi s_\phi & c_\psi c_\phi & -s_\psi \\ -s_\theta c_\phi + s_\psi c_\theta s_\phi & s_\theta s_\phi + s_\psi c_\theta c_\phi & c_\psi c_\theta \end{bmatrix}
\end{aligned}
\tag{1}
$$

The location of the spherical joints, A_i, can be defined as (constant) components in the mobile frame as:

$$
\begin{aligned}
\mathbf{a}'_1 &= \left[a'_{1x}, a'_{1y}, a'_{1z}\right]^T = \left[r_p, 0, 0\right]^T \\
\mathbf{a}'_2 &= \left[a'_{2x}, a'_{2y}, a'_{2z}\right]^T = \left[r_p c_{\beta_2}, r_p s_{\beta_2}, 0\right]^T \\
\mathbf{a}'_3 &= \left[a'_{3x}, a'_{3y}, a'_{3z}\right]^T = \left[r_p c_{\beta_3}, r_p s_{\beta_3}, 0\right]^T
\end{aligned}
\tag{2}
$$

and as $\mathbf{a}_i = \mathbf{p} + \mathbf{T}\mathbf{a}'_i$ in the fixed frame, with individual expressions defined as follows:

$$
\begin{aligned}
a_{ix} &= x + T_{11}a'_{ix} + T_{12}a'_{iy} + T_{13}a'_{iz} \\
a_{iy} &= y + T_{21}a'_{ix} + T_{22}a'_{iy} + T_{23}a'_{iz} \\
a_{iz} &= z + T_{31}a'_{ix} + T_{32}a'_{iy} + T_{33}a'_{iz}
\end{aligned}
\tag{3}
$$

Using the assumptions listed previously and the above vector loop equations, a closed form linear solution is possible from a set of 3 constraint equations (composed of both the known and unknown task-space variables):

$$
\begin{aligned}
a_{1y} &= y + T_{21}r_p = 0 \\
a_{2y} &= a_{2x}\tan(\beta_2) \\
a_{3y} &= a_{3x}\tan(\beta_3)
\end{aligned}
\tag{4}
$$

which when substituting components from equations (1–3), can be solved for the unknown task-space variables directly, the result of which describes the full pose of the mobile platform in Cartesian Space. For completeness, the equation set is included here:

$$
\begin{aligned}
\phi &= \tan^{-1}\left[\frac{-((c_{\beta_2} - c_{\beta_3})(c_\theta - c_\psi) + (s_{\beta_2} - s_{\beta_3})s_\theta s_\psi)}{(c_{\beta_2} - c_{\beta_3})s_\theta s_\psi - (s_{\beta_2} - s_{\beta_3})c_\theta + \left(\frac{c_{\beta_3} - 1}{t_{\beta_3}} - \frac{c_{\beta_2} - 1}{t_{\beta_2}}\right)c_\psi}\right] \\
x &= -r_p(c_\theta c_\phi + s_\psi s_\theta s_\phi)c_{\beta_2} - r_p(-c_\theta s_\phi + s_\psi s_\theta c_\phi)s_{\beta_2} \\
&\quad + \frac{r_p}{t_{\beta_2}}(c_\psi s_\phi(c_{\beta_2} - 1) + c_\psi c_\phi s_{\beta_2}) \\
y &= -c_\psi s_\phi r_p.
\end{aligned}
$$

2.2.2. Forward Displacement Solution (FDS)

Conversely to the IDS, the purpose of the 3-RPS FDS is to determine the pose of the mobile platform from a given set of prismatic joint positions. Again, as was the case for the ideal IDS, the ideal 3-RPS FDS is identical to the 3-PRS developed in [20], also making use of the assumptions listed in Section 2.2.1.

In this case, since the intersection point of the revolute joint axes and the prismatic joint lines of action (*i.e.*, B_i) are known and the prismatic joint lengths (*i.e.*, q_i for i=1,2,3) are provided as input, the spherical joints (A_i) must lie on a circle of radius q_i centred on B_i. Using this information and the vector loop equation ($\mathbf{q}_i = \mathbf{a}_i - \mathbf{b}_i$), the square of length of the i-th leg can be expressed as:

$$
q_i^2 = (a_{ix} - b_{ix})^2 + (a_{iy} - b_{iy})^2 + (a_{iz} - b_{iz})^2
$$

The result is a set of 3 non-linear functions composed of known manipulator geometry, 3 unknown independent task-space variables and 3 dependent task-space variables. While it should be noted that Tsai *et al.* show that an analytical solution is possible for the FDS [17], it is known to result in 16 different solutions for this manipulator with identification of the desired solution providing its own challenges. Instead, as was the case for [16], a numerical approach using the Levenberg-Marquardt (L-M) algorithm was used by first estimating the three independent task-space variables (based on the provided prismatic joint positions), and then completing a local search to obtain the full pose of the mobile platform directly.

2.3. Extended Kinematic Model

As detailed in Section 2.2.1, a number of assumptions were required to solve both the inverse and forward displacement problems of the 3-RPS with the methods described in their respective sections. However, these
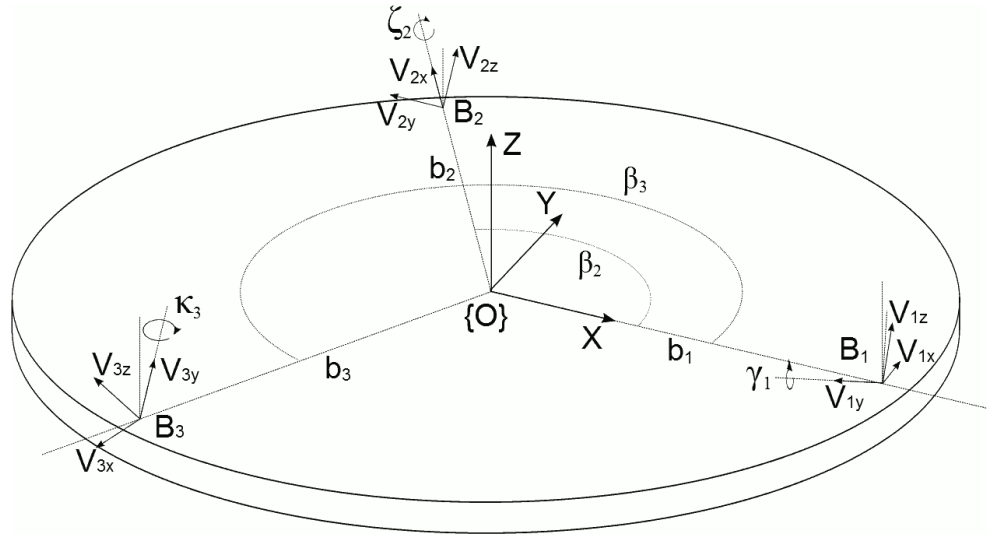
Fig. 2. Extended kinematic model error angles.

assumptions are not necessarily valid and only partially reflective of the actual manipulator kinematics at best. Nor are these assumptions required to obtain solutions to these problems, they simply need to be replaced with variables describing the particular ideal model deviation and included in the very same vector additions used previously, namely $\mathbf{q}_i = \mathbf{a}_i - \mathbf{b}_i$.

To begin, the angles β_i at the base and mobile platform frame need not be the same. To address this assumption, an independent angle set is introduced describing the spherical joint locations in $\{O'\}$, α_i. The next assumption to be addressed is that all points B_1, B_2 and B_3 lie on a circle of radius r_b centred on the base link frame. While it is convenient to affix $\{O\}$ to this circle centre and align the X-axis to contain B_1, due to machining/assembly errors, the circle is unlikely to also contain the remaining intersection points with nominal radius r_b. To correct for this, each point B_i will be located at its own respective radial position, namely r_{bi}, relative to O. Similarly, for the mobile platform and the spherical joint locations, A_i, to be located at their respective radial positions, r_{pi}.

Further, it is assumed that the fixed base revolute joint axes are simultaneously perpendicular to $\mathbf{b}_i$ and co-planar to the base link frame X-Y plane, both of which are highly unlikely for even the most well made of mechanisms. Realistically, achievable machining and assembly tolerances preclude this assumed perfection and to reflect this, two angles for each branch are introduced to capture these misalignments. As shown in Fig. 2, for a local coordinate system $\{V_i\}$ located at B_i, the first rotation ζ_i represents a rotation of this coordinate system about an axis parallel to $\mathbf{b}_i$, allowing for the revolute joint to be skewed with respect to the base link X-Y plane (this includes a $\pi/2$ rotation to align the frame's Z-axis with the revolute joint axis). The second rotation, κ_i, represents a rotation about the frame's Y-axis (*i.e.*, V_{iy}), removing the requirement for the revolute joint axis to be perpendicular to $\mathbf{b}_i$.

As well and for the same reasons described above, the assumption that the line of action of the prismatic joint is perpendicular to the revolute joint axis is also highly unlikely. For this angle γ_i is introduced describing a rotation about the rotated Y-axis (V_{iy}).

Finally, as was the case in [16] and demonstrated in [18], the errors associated with imperfect spherical joints are regarded as negligible relative to other joint errors and continue to be assumed ideal for this extended kinematic model. Based on these assumptions, the number of independent kinematic parameters total 34 and are summarized in Table 1. Note that, while it is possible to reduce the parameter set further by co-locating $\{O\}$ at B_1, r_{b1} is included for clarity and ease of implementation.

Branch 1	r_{b1}	r_{p1}	ζ_1	κ_1	γ_1	δq_1		
Branch 2	r_{b2}	r_{p2}	ζ_2	κ_2	γ_2	δq_2	α_2	β_2
Branch 3	r_{b3}	r_{p3}	ζ_3	κ_3	γ_3	δq_3	α_3	β_3
External Measurement - Fixed Base	X_B	Y_B	Z_B	ψ_B	θ_B	ϕ_B		
External Measurement - Platform	X_P	Y_P	Z_P	ψ_P	θ_P	ϕ_P		

Table 1. Summary of kinematic parameters in the extended model.

From [19], it is shown that the minimum number of kinematic parameters required to completely define a parallel manipulator can be obtained by:

$$N_T = 3R + P + 2C + SI + E + 6L + 6(F-1)$$

where R the total number of revolute joints, P is the total number of prismatic joints, C is the total number of cylindrical joints, SI is the total number of 'singular' links (*e.g.*, SS link), E is the total number of encoders (or other joint sensor), L is the number of independent kinematic loops and F is the number of arbitrary reference frames. For the 3-RPS, this equation results in:

$$N_T = 3(3) + 3 + 2(0) + (0) + 3 + 6(2) + 6(2-1) = 33. \tag{5}$$

2.3.1. Augmented Constraint Equations

As was the case for the ideal model, the basis for the constraint equations used in both the extended IDS and FDS are the same vector loops depicted earlier in Fig. 1. While equation (3) is written in its general form and still applies, equation (2) requires an update to include the expanded parameter set as follows:

$$\mathbf{a}_i' = \begin{bmatrix} r_{pi}cos(\alpha_i) \\ r_{pi}sin(\alpha_i) \\ 0 \end{bmatrix}$$

Additional vector definitions required include $\mathbf{b}_i$ and $\mathbf{q}_i'$ describing the location of B_i (in $\{O\}$) and the location of A_i (in $\{V_i\}$) respectively:

$$\mathbf{b}_i = \begin{bmatrix} r_{bi}cos(\beta_i) \\ r_{bi}sin(\beta_i) \\ 0 \end{bmatrix} \qquad \mathbf{q}_i' = \begin{bmatrix} 0 \\ 0 \\ q_i \end{bmatrix}$$

which, when rotated to the base link frame, define two separate vector loops describing the locations of each branch's respective spherical joint, A_i, as follows:

$$\begin{aligned} \mathbf{a}_i &= \mathbf{b}_i + \mathbf{R}_z(\beta_i)\mathbf{R}_x(\pi/2 + \zeta_i)\mathbf{R}_y(\kappa_i)\mathbf{R}_z(\lambda_i)\mathbf{R}_y(\pi/2 + \gamma_i)\mathbf{q}_i' \\ \mathbf{a}_i &= \mathbf{p} + \mathbf{R}_y(\theta)\mathbf{R}_x(\psi)\mathbf{R}_z(\phi)\mathbf{a}_i' \end{aligned}$$

Subtracting the two equations results in a set of 9 non-linear equations (3 for each branch) which are functions of known manipulator geometry, 3 specified input parameters and 9 unknowns. Exactly which variables are specified and which are unknown depend on whether the IDS or FDS will be employed.

2.3.2. Extended Model IDS

In the case of the extended IDS, input to the problem would be three of the six task space variables, for example $[z, \psi, \theta]$, leaving $[x, y, \phi, q_1, q_2, q_3, \lambda_1, \lambda_2, \lambda_3]$ as unknowns in that case. Once the inputs and unknowns have been defined, the equations are then solved numerically using a multi-variable local search algorithm (Levenberg-Marquardt with exact Jacobian). This results in a description of the full pose of the mobile platform.

2.3.3. Extended Model FDS

Conversely for the extended FDS, input to the problem would be the set of prismatic joint positions $[q_1, q_2, q_3]$, leaving $[x, y, z, \psi, \theta, \phi, \lambda_1, \lambda_2, \lambda_3]$ as problem unknowns. As was the case for the IDS, again the FDS is solved numerically using the same L-M algorithm to arrive at the full pose of the mobile platform, thereby completing the FDS.

3. PARAMETRIC STUDY AND DISCUSSION

So as to better understand the significance of the various model errors and their effect on overall deviation between the extended model and the ideal model, a parametric study was performed systematically varying each of the available error parameters and comparing the sum L-2 norms of the displaced spherical joints. For demonstration purposes, error parameter effects were evaluated in two different manipulator configurations: 1) a neutral position with all prismatic joint positions equal, all error parameters zero except the parameter under test and 2) a tipped/tilted orientation with an imposed random small error set applied (but consistent throughout test) at each branch, all branch lengths different.

As well, tests were performed to evaluate the performance of the L-M local search algorithm. In these tests, the results of the L-M algorithm were compared to the exact analytical solution of the ideal model (with all error parameters zero) as well as an assessment of how well a particular input to the extended model IDS (for example $[z, \psi, \theta]$) can be returned via the extended model FDS using the extended model IDS output.

For test purposes the fixed and mobile platforms used in the simulations were 2 m and 1 m in diameter respectively. Also note that, in order to demonstrate the effect of each error parameter, some variables were expanded to include a nominal component and an error component as follows:

$$
\begin{aligned}
r_{bi} &= r_b + \delta r_{bi} & (6) \\
r_{pi} &= r_p + \delta r_{pi} & (7) \\
\alpha_i &= \alpha_i + \delta \alpha_i & (8) \\
\beta_i &= \beta_i + \delta \beta_i & (9)
\end{aligned}
$$

3.1. Levenberg-Marquardt Local Search

To assess how well the L-M algorithm performs as compared to the analytical solution in comparative configurations (*i.e.*, all error parameters zero), 1000 random inputs to both the extended and ideal IDS were processed and compared. As shown in Fig. 3(a), the mean error was 2.21×10^{-9} m with a min/max and range of 1.65×10^{-10} / 1.32×10^{-8} m and 1.31×10^{-8} m respectively. Since the solution of the ideal model IDS is exact, this result represents the limit of the L-M algorithm accuracy for the given optimization loop termination criteria (2.2×10^{-16} m).

A second test to compare the algorithm's ability to return a given input after being processed via the complementary solution was also evaluated. To accomplish this, 1000 sets of random (*i.e.*, $[z, \psi, \theta]$) inputs were sent to the extended model IDS, upon which the output was subsequently sent to the extended model FDS as input to arrive back at the original $[z, \psi, \theta]$ inputs. In this case, as expected given back-to-back numerical solutions, both the mean error (6.06×10^{-9} m) and range (1.22×10^{-7} m) were higher when compared to the above results. See Fig. 3(b) for details.

3.2. Test Case 1: All prismatic joint positions equal, error parameters zero.

The first of the manipulator configurations analysed was as shown in Fig. 1 with all prismatic joints equal (1.956 m), all error parameters equal to zero and all joints separated by $120°$. From there, each error parameter was varied through a range of $\pm 2.5°$ for angles and ± 1.3 mm for displacements to assess their
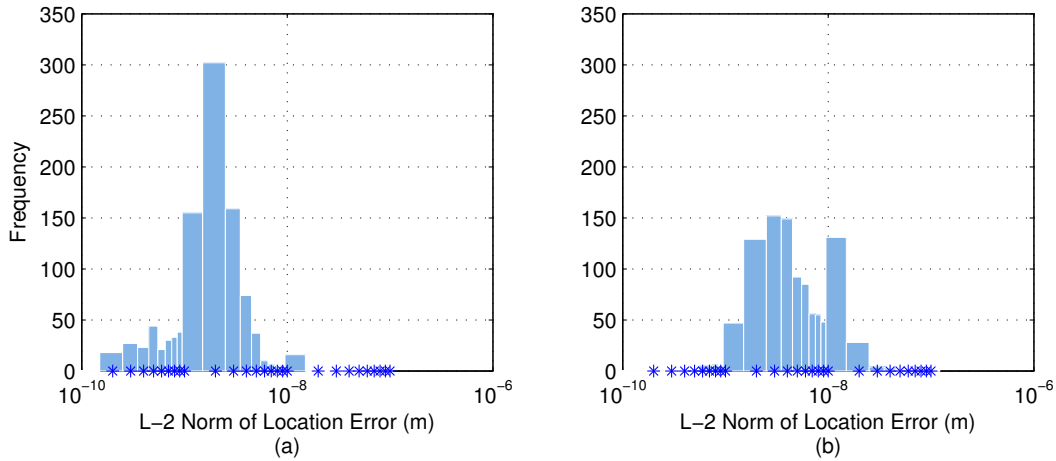
Fig. 3. Norm of spherical joint location error: (a) Extended *vs*. Ideal IDS, (b) IDS input *vs*. FDS output.
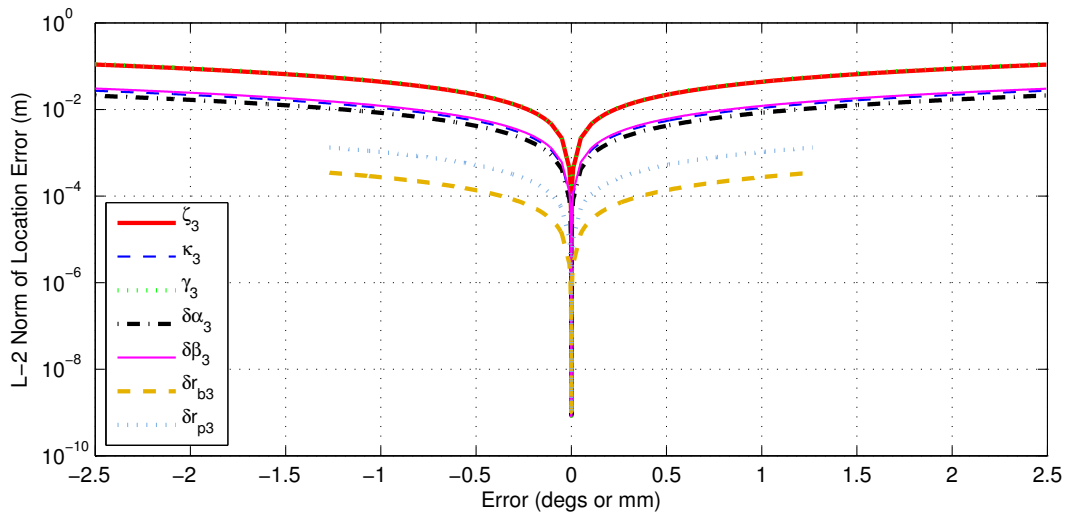
Fig. 4. Case 1 (no errors): Branch 3 parameter variation results.

effect on spherical joint location error as compared to the ideal solution. From the overlaid plots in Fig. 4, error parameters γ_i and ζ_i induce the most significant deviation from the ideal model , however errors related to κ_i, $\delta\beta_i$ and $\delta\alpha_i$ also appear significant for the scale of the manipulator. Note that in the absence of any other error angles, effects from γ_i, ζ_i and κ_i, $\delta\beta_i$ are indistinguishable from each other, and why their plots appear as identical in this configuration. Also note that as the error angles approach zero, the extended model approaches the ideal model its being compared to and results in the sharp drop in spherical joint location error seen near the origin of the plot. For brevity, only the results from Branch 3 are shown, however identical results were obtained for the remaining two branches.

3.3. Test Case 2: Tipped/Tilted configuration with a full set of random error angles.

The second manipulator configuration analysed was as shown in Fig. 5a with each prismatic joint at a unique position (1.778 m, 2.159 m, and 1.956 m), all joints were separated by 120° and with a random set of error parameters applied as specified in Fig. 5b. From there, each error parameter was varied through a range of $\pm 2.5°$ for angles and ± 1.3 mm for displacements to assess their effect on spherical joint location error as
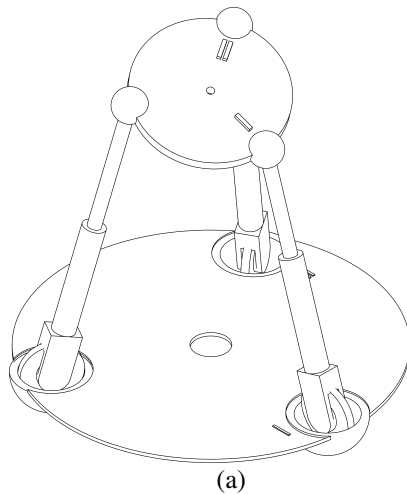
	ζ	κ	γ	$\delta\alpha$	$\delta\beta$	δr_p	δr_b
Branch 1	-1.97	-1.49	-1.58	N/A	N/A	N/A	N/A
Branch 2	1.37	-1.05	1.00	1.29	0.78	0.9	-1.2
Branch 3	1.06	-0.6	1.68	1.47	0.86	-0.6	-0.9

<div style="text-align:center">(a)   (b)</div>

Fig. 5. Case 2: (a) Manipulator configuration and (b) Error angle/distance set for parameter variation testing (angles = degs, distance = mm).

compared to the ideal solution. From the overlaid plots in Figures 6 (a), (b) and (c) , again error angles γ_i and ζ_i typically induce the most significant deviations from the ideal model, however errors related to κ_i and $\delta\beta_i$) continue to be significant for the scale of the manipulator. Another important conclusion arising from these plots is that decreasing any particular error parameter does not necessarily improve the overall spherical joint location error. For all the configurations tested so-far, whether or not increasing /decreasing any particular error parameter improves/worsens the overall spherical joint location error has been dependent on the entire set of parameters.

4. CONCLUSIONS

The 3-RPS spatial parallel manipulator was introduced and subsequently analysed to develop both the ideal and extended kinematic models. As part of this process, the ideal model inverse displacement and forward displacement solutions were presented and used as a basis for comparison. Following this, the extended model inverse and forward displacement solutions were also presented and used as the basis for detailed parameter variation testing. For these tests, the effect each error angle has on the overall spherical joint location error was evaluated at each branch for two different manipulator poses. Testing was also performed on the accuracy of the L-M local search optimization algorithm used to solve the non-linear equation sets. The metric for assessing overall displacement error was to sum the L-2 Norms of the resulting spherical joint location displacements as compared to a reference position (which is test dependent).

The first test case analysed had the mobile platform at zero rotational / X-Y axes displacements and a 1.891 m Z displacement from the fixed base link frame. In this configuration, each error parameter was varied through a range of $\pm2.5°$ for angles and ±1.3 mm for displacements to demonstrate the effect on overall spherical joint location error. From the resulting plots it was seen that in this configuration, error parameters γ_i and ζ_i induced the most significant deviation from the ideal model. However, errors related to κ_i, $\delta\beta_i$ and $\delta\alpha_i$ were also shown to be significant for the scale of the manipulator. It was also noted that in this case, with all other error parameters being zero while not under test, γ_i, ζ_i and κ_i, $\delta\beta_i$ were indistinguishable from each other in their effect.

The second test case analysed had the mobile platform rotated/displaced in every axis as compared to test case 1 with the addition of a complete set of error inputs prior to parameter variation. In this configuration, again each error parameter was varied through a range of $\pm2.5°$ for angles and ±1.3 mm for displacements
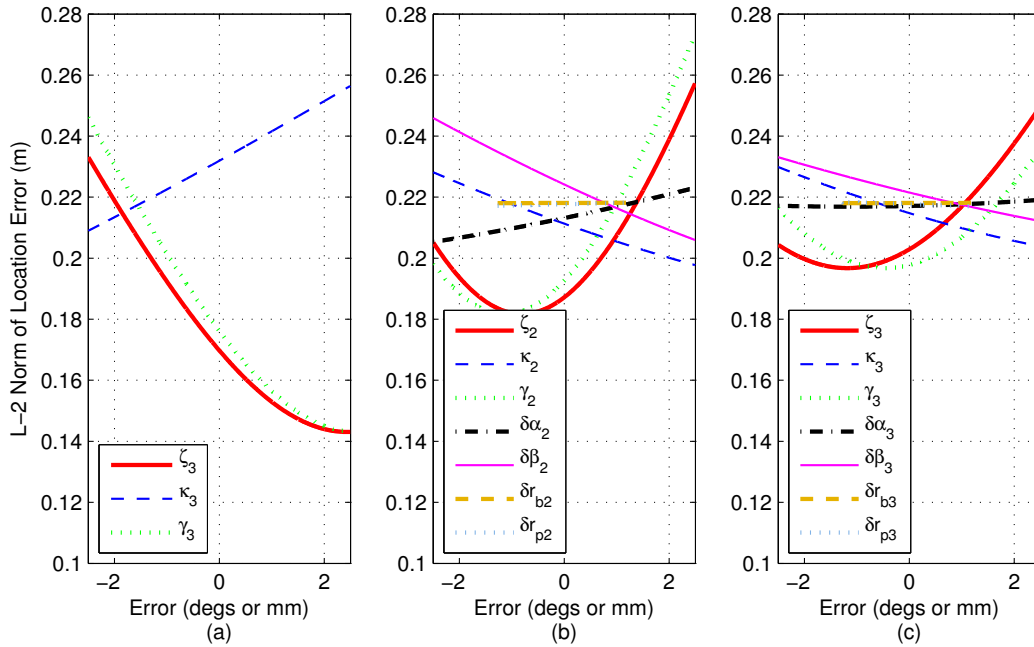
Fig. 6. Case 2 (with errors) parameter variation results: (a) Branch 1, (b) Branch 2, (c) Branch 3.

to demonstrate the effect on overall spherical joint location error. From the resulting plots it was seen that in this configuration, again error angles γ_i and ζ_i typically induced the most significant deviations from the ideal model, however errors related to κ_i and $\delta\beta_i$ continued to be significant for the scale of the manipulator. It was also seen from these tests that decreasing any particular error angle does not necessarily improve the overall spherical joint location error.

Testing of the L-M algorithm accuracy was also completed to help explain the limits of the employed techniques. To this end, two tests were completed; 1) evaluating comparable configurations using both the exact solution and the L-M numerical approach and 2) determining how well the L-M numerical IDS/FDS solutions can return the original input when evaluated back-to-back (*i.e.*, IDS results fed to FDS input). As expected, comparison errors to the exact solution are lower than comparison errors to a secondary numerical process, however, comparison errors in both cases were low and on the order of 10^{-8} m.

REFERENCES

1. V. E. Gough, S. G. Whitehall, "Universal Tyre Test Machine", *Proceedings of 9th International Congress of F.I.S.I.T.A*, 117, pp. 117-135, 1962.
2. D. Stewart, "A Platform With Six Degrees of Freedom", *Proceedings of the Institute of Mechanical Engineering*, Vol. 180, pp. 371-386, 1965.
3. R. B. Aronson, "A bright horizon for machine tool technology", *Manufacturing Engineering*, 116, pp. 57-70, 1996.
4. M. Glavonjic, D. Milutinovic, S. Zivanovic, Z. Dimic, V. Kvrgic, "Desktop 3-axis parallel kinematic milling machine", *International Journal of Manufacturing Technology*, 46, pp. 51-60, 2010.
5. J. Arata, H. Kondo, N. Ikedo, H. Fujimoto, "Haptic Device Using a Newly Developed Redundant Parallel Mechanism", *IEEE Transactions on Robotics*, Vol. 27, No. 2, pp. 201-214, 2011.
6. K. H. Hunt, "Structural Kinematics of In-Parallel-Actuated Robot-Arms", *Journal of Mechanisms, Transmissions and Automation in Design*, Vol. 105, pp. 705-712, 1983.

7. C. H. Liu, S. Cheng, "Direct Singular Positions of 3RPS Parallel Manipulators", *Journal of Mechanical Design*, Vol. 126, pp. 1006-1016, November 2004.

8. S. A. Joshi, L.-W. Tsai, "Jacobian Analysis of Limited-DOF Parallel Manipulators", *Journal of Mechanical Design*, Vol. 124, pp. 254-258, June 2002.

9. L. Notash, R. P. Podhorodeski, "On the Forward Displacement Problem of Three-Branch Parallel Manipulators", *Mechanism and Machine Theory*, Vol. 30, No. 3, pp. 391-404, 1995.

10. A. Sokolov, P. Xirouchakis, "Dynamic analysis of a 3-DOF parallel manipulator with R-P-S joint structure", *Mechanism and Machine Theory*, Vol. 42, pp. 541-557, 2007.

11. J. A. Carretero, R. P. Podhorodeski, M. A. Nahon and C. M. Gosselin, "Kinematic analysis and optimization of a new three degree-of-freedom spatial parallel manipulator", *Journal of Mechanical Design*, Vol. 122, pp. 17-24, March 2000.

12. N. M. Rao, K. M. Rao, "Dimensional synthesis of a spatial 3-RPS parallel manipulator for a prescribed range of mtion of spherical joints", *Mechanism and Machine Theory*, Vol. 44, pp. 477-486, March 2009.

13. Y. Lu, T. Leinonen, "Solution and Simulation of Position-Orientation for Multi-Spatial 3-RPS Parallel Mechanisms in Series Connection", *Multibody System Dynamics*, Vol. 14, pp. 47-60, 2005.

14. K.-M. Lee, D. K. Shah, "Kinematic Analysis of a Three-Degrees-of-Freedom In-Parallel Actuated Manipulator", *IEEE Journal of Robotics and Automation*, Vol. 4, No. 3, pp. 354-360, June 1988.

15. J. Xiong, X. Han, W. Chen, "Study on the Accuracy of 3-RPS Parallel Machine Tools", *Key Engineering Materials*, Vols. 407-408, pp. 89-93, 2009.

16. S. M. O'Brien and J. A. Carretero, "Augmented model of the 3-PRS manipulator for kinematic calibration", in "Advances in Robotic Kinematics: Analysis and Design", Batz-sur-Mer, France, 2008.

17. L.-W. Tsai, *Robot Analysis*, 1 ed.. John Wiley & Sons, Inc, 1999.

18. O. Masonry, J. Wang and H. Zhuang, "Kinematic modeling and calibration of a stewart platform", *Journal of Advanced Robotics*, Vol. 11, No. 5, pp. 519-539, 1997.

19. I. Fassi and G. Legnani, "Automatic identification of a minimum, complete and parametrically continuous model for geometric calibration of parallel robots", *Proceedings of the Workshop on Fundamental Issues and Future Research Directions for Parallel Mechanisms and Manipulators*, Quebec City, Quebec, October 3-4, 2002.

20. M.-S. Tsai, T.-N. Shiau, Y.-J. Tsai and T.-H. Chang, "Direct kinematic analysis of a 3-PRS parallel machanism", *Mechanism and Machine Theory*, Vol. 38, pp. 71-83, 2003.